

Kinetic theory description of liquid-vapour flows using the Enskog-Vlasov model

S. Busuioc and L. Gibelli

School of Engineering, The University of Edinburgh, Edinburgh, EH9 3FB,
United Kingdom

Departement of Physics, West University of Timișoara, Bd. Vasile Pârvan 4,
300223 Timișoara, Romania

19th of May 2022



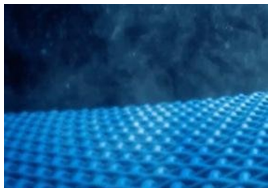
Ubiquitous nature of fluid flows with phase change



Cometary atmospheres.



Laser induced
vaporisation of solids.



Capillary cooling of
electronic devices.

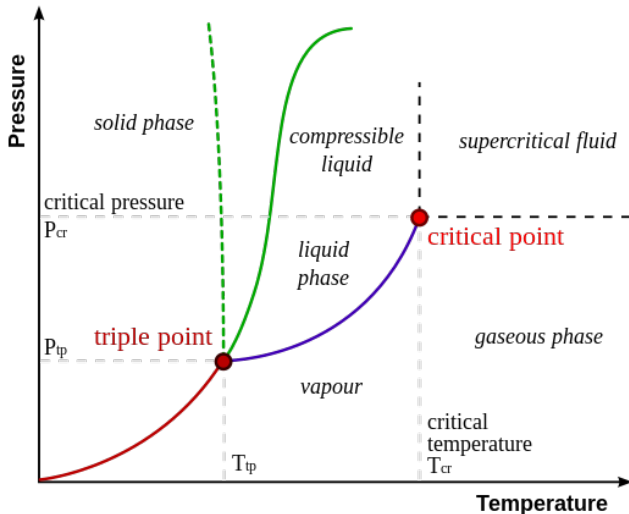


Diesel fuel droplet
dynamics.

- 1 The Enskog-Vlasov model
- 2 Evaporation of monoatomic gases - origin of temperature anisotropy in the distribution of evaporated molecules
- 3 Evaporation of polyatomic gases - distribution function of evaporated molecules
- 4 Enskog-Vlasov in spherical geometry - growth of droplets in superheated/supercooled vapor and bubbles in superheated liquid

The Enskog-Vlasov equation (I)

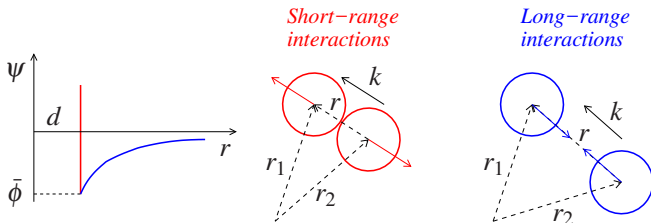
- Unlike the Boltzmann equation, the Enskog-Vlasov equation has the capability of handling both the liquid and vapor phases.



The Enskog-Vlasov equation (I)

- Let us consider a system of particles of mass m and diameter d .
- Let us assume that interactions between particles occur through the Sutherland potential:

$$\phi(\rho) = \begin{cases} +\infty, & \rho < a, \\ -\phi_a \left(\frac{\rho}{a}\right)^{-\gamma}, & \rho \geq a, \end{cases} \quad (1)$$



The Enskog-Vlasov equation (II)

- The dynamics of the system of particles can be described by the following exact kinetic equation:

$$\frac{\partial f}{\partial t} + \mathbf{v} \cdot \nabla_{\mathbf{r}} f = \frac{1}{m} \nabla_{\mathbf{v}} \cdot \left\{ \int_{\mathbb{R}^3} d\mathbf{v}_* \int_{r>d} d\mathbf{r}_* \frac{d\phi}{dr} f_2(\mathbf{r}, \mathbf{v}, \mathbf{r}_*, \mathbf{v}_*) \hat{\mathbf{k}} \right\} + a^2 \int_{\mathbb{R}^3} d\mathbf{v}_* \int_{S_+} d^2 \hat{\mathbf{k}} \left\{ f_2(\mathbf{r}, \mathbf{v}', \mathbf{r} + a \hat{\mathbf{k}}, \mathbf{v}') - f_2(\mathbf{r}, \mathbf{v}, \mathbf{r} - a \hat{\mathbf{k}}, \mathbf{v}_*) \right\} (\mathbf{v}_r \cdot \hat{\mathbf{k}}).$$

- Let us now make the following *simplifying* assumptions:
 - Long-range correlations are neglected:

$$f_2(\mathbf{r}, \mathbf{v}, \mathbf{r}_*, \mathbf{v}_*, t) = f(\mathbf{r}, \mathbf{v}, t) f(\mathbf{r}_*, \mathbf{v}_*, t).$$

- Short-range correlations are taken into account as in Enskog theory:

$$f_2(\mathbf{r}, \mathbf{v}, \mathbf{r} \pm d \hat{\mathbf{k}}, \mathbf{v}_*, t) = \chi \left[n \left(\mathbf{r} \pm \frac{a}{2} \hat{\mathbf{k}} \right) \right] f(\mathbf{r}, \mathbf{v}, t) f(\mathbf{r} \pm a \hat{\mathbf{k}}, \mathbf{v}_*, t).$$

where χ is the contact value of the pair correlation function of a hard sphere fluid.

- Non-local collision are natural when dealing with non-punctiform particles

The Enskog-Vlasov equation (III)

- Different expression of the contact value of the pair correlation function can be used:
- **Standard Enskog Theory (SET)**: value of the pair correlation function in a fluid in *uniform equilibrium* with density at the contact point.

$$\chi = \chi_{\text{SET}} \left(n \left(\mathbf{r} \pm \frac{a}{2} \hat{\mathbf{k}} \right) \right) = \frac{1}{nb} \left(\frac{p^{CS}}{nk_B T} - 1 \right) = \frac{1}{2} \frac{2 - \eta}{(1 - \eta)^3}; \quad b = \frac{2\pi a^3}{3}; \quad \eta = \frac{\pi a^3 n}{6}.$$

where p^{CS} is given by:

$$p^{CS} = \frac{1 + \eta + \eta^2 - \eta^3}{(1 - \eta)^3} \quad (2)$$

The Enskog-Vlasov equation (III)

- Different expression of the contact value of the pair correlation function can be used:
- **Revised Enskog Theory (RET)**: value of the pair correlation function in a fluid in *non-uniform equilibrium* with density at the contact point.

$$\text{Fischer-Methfessel approximation} \quad \rightsquigarrow \quad \chi = \chi_{\text{RET-FM}} \left[n \left(\mathbf{r} \pm \frac{a}{2} \hat{\mathbf{k}} \right) \right] = \chi_{\text{SET}} \left(\bar{n} \left(\mathbf{r} \pm a \frac{\hat{\mathbf{k}}}{2} \right) \right).$$

where

$$\bar{n}(\mathbf{r}, t) = \frac{3}{4\pi a^3} \int_S n(\mathbf{r}_1, t) w(\mathbf{r}, \mathbf{r}_1) d\mathbf{r}_1, \quad w(\mathbf{r}, \mathbf{r}_1) = \begin{cases} 1, & \|\mathbf{r}_1 - \mathbf{r}\| < a \\ 0, & \|\mathbf{r}_1 - \mathbf{r}\| > a \end{cases}.$$

The Enskog-Vlasov equation (IV)

- The above simplifying assumptions lead to the following *closed* kinetic equation, which is referred to as Enskog-Vlasov equation^{1,2,3,4}:

$$\frac{\partial f}{\partial t} + \mathbf{v} \cdot \nabla_{\mathbf{r}} f + \underbrace{\frac{\mathbf{F}(\mathbf{r})}{m} \cdot \nabla_{\mathbf{v}} f}_{\text{Vlasov term}} = \underbrace{\mathbf{C}(f, f)}_{\text{Enskog term}}$$

$$\mathbf{F}(\mathbf{r}) = \int_{r>a} d\mathbf{r}_* \frac{1}{r} \frac{d\phi}{dr} (\mathbf{r}_* - \mathbf{r}) n(\mathbf{r}_*),$$

$$\mathbf{C}(f, f) = a^2 \int_{\mathbb{R}^3} d\mathbf{v}_* \int_{S_+} d^2 \hat{\mathbf{k}} \left\{ \chi_{\text{SET}}[\bar{n}(\mathbf{r} - a/2\mathbf{k})] f(\mathbf{r}, \mathbf{v}') f(\mathbf{r} + a\hat{\mathbf{k}}, \mathbf{v}_*) - \chi_{\text{SET}}[\bar{n}(\mathbf{r} - a/2\mathbf{k})] f(\mathbf{r}, \mathbf{v}) f(\mathbf{r} - a\hat{\mathbf{k}}, \mathbf{v}_*) (v_r \cdot \hat{\mathbf{k}}) \right\}.$$

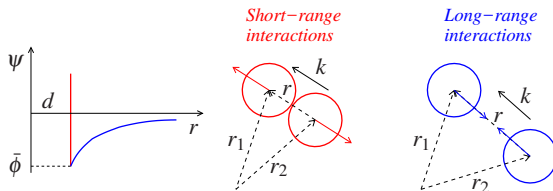
¹ L. De Sobrino, *Can. J. Phys.* 45 (2), 363-385 (1967).

² M. Grmela, *J. Stat. Phys.* 3 (3), 347-364 (1971).

³ J. Karkheck, G. Stell, *J. Chem. Phys.* 75 (3), 1475-1487 (1981).

⁴ A. Frezzotti, L. Gibelli, S. Lorenzani, *Phys. Fluids* 17, 012012 (2005).

The Enskog-Vlasov equation (IV)



$$\frac{\partial f}{\partial t} + \mathbf{v} \cdot \nabla_{\mathbf{r}} f + \underbrace{\frac{\mathbf{F}(\mathbf{r})}{m} \cdot \nabla_{\mathbf{v}} f}_{\text{Vlasov term}} = \underbrace{\mathbf{C}(f, f)}_{\text{Enskog term}}$$

$$\mathbf{F}(\mathbf{r}) = \int_{r>a} d\mathbf{r}_* \frac{1}{r} \frac{d\phi}{dr} (\mathbf{r}_* - \mathbf{r}) n(\mathbf{r}_*),$$

$$\mathbf{C}(f, f) = a^2 \int_{\mathbb{R}^3} d\mathbf{v}_* \int_{\mathcal{S}_+} d^2 \hat{\mathbf{k}} \left\{ \chi_{\text{SET}}[\bar{n}(\mathbf{r} - a/2\mathbf{k})] f(\mathbf{r}, \mathbf{v}') f(\mathbf{r} + a\hat{\mathbf{k}}, \mathbf{v}_*) - \chi_{\text{SET}}[\bar{n}(\mathbf{r} - a/2\mathbf{k})] f(\mathbf{r}, \mathbf{v}) f(\mathbf{r} - a\hat{\mathbf{k}}, \mathbf{v}_*) (v_r \cdot \hat{\mathbf{k}}) \right\}.$$

¹ L. De Sobrino, *Can. J. Phys.* 45 (2), 363-385 (1967).

² M. Grmela, *J. Stat. Phys.* 3 (3), 347-364 (1971).

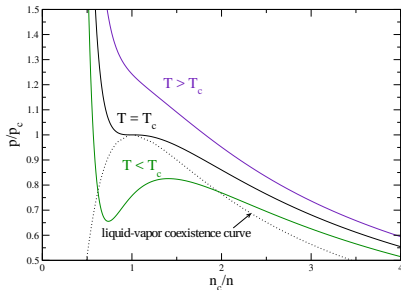
³ J. Karkheck, G. Stell, *J. Chem. Phys.* 75 (3), 1475-1487 (1981).

⁴ A. Frezzotti, L. Gibelli, S. Lorenzani, *Phys. Fluids* 17, 012012 (2005).

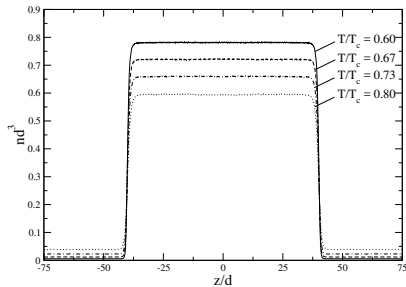
Liquid-vapour coexistence curve for simple liquids

- Equation of state of the fluid described by the Enskog-Vlasov equation has a generalised van der Waals form:

$$p_0(n, T) = nkT \underbrace{\frac{1 + \eta + \eta^2 - \eta^3}{(1 - \eta)^3}}_{\text{repulsive interactions}} - \underbrace{\frac{2\pi a^3}{3} \frac{\gamma}{\gamma - 3} \phi_a n^2}_{\text{attractive interactions}}, \quad \rightsquigarrow \quad \begin{aligned} T_c &\approx 0.094 \frac{4\gamma}{\gamma - 3} \frac{\phi_a}{k} \\ \eta_c &\approx 0.13 \end{aligned}$$



(a) Phase diagram.



(b) Density profiles.

The Enskog-Vlasov equation: Fluid-dynamic description

- The Enskog-Vlasov equation leads to the following fluid dynamics equations:

$$\partial_t (\rho) + \nabla \cdot (\rho \mathbf{u}) = 0 \quad ,$$

$$\partial_t (\rho \mathbf{u}) + \nabla \cdot (\rho \mathbf{u} \mathbf{u} + \mathbf{\Pi}) = 0 \quad ,$$

$$\partial_t \left[\left(\rho e + \frac{1}{2} \rho u^2 + \kappa |\nabla \rho|^2 \right) \right] + \nabla \cdot \left[\mathbf{u} \left(\rho e + \frac{1}{2} \rho u^2 + \kappa |\nabla \rho|^2 \right) + \mathbf{\Pi} \cdot \mathbf{u} + \mathbf{q} \right] = 0,$$

where $\kappa = \frac{2}{15} \frac{\gamma}{\gamma-5} \phi_a a^5$.

- “Korteweg” contributions appear in the expressions of the stress tensor and heat flux:

$$\mathbf{\Pi} = \left(p_0 - \kappa \rho \nabla^2 \rho - \frac{\kappa}{2} |\nabla \rho|^2 \right) \mathbf{I} - \mu (\nabla \mathbf{u} + \nabla \mathbf{u}^\top) - \lambda (\nabla \cdot \mathbf{u}) \mathbf{I} + \kappa \nabla \rho \nabla \rho,$$

$$\mathbf{q} = -k \nabla T + \kappa \rho (\nabla \cdot \mathbf{u}) \nabla \rho.$$

¹ D.M. Anderson, G.B. McFadden, A.A. Wheeler, *Ann. Rev. Fluid Mech.* 30 (1), 139-165 (1998).

² X. He, G.D. Doolen, *J. Stat. Phys.* 107 (1), 309-328 (2002).

The Enskog-Vlasov DSMC-like method^{1,2}

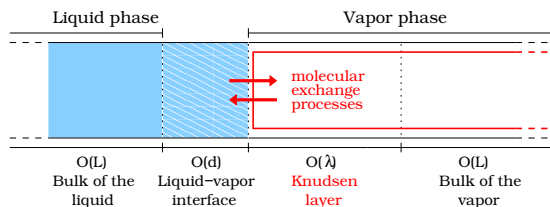
In Cartesian coordinates, the components of the self-consistent force field normal direction to the vapor-liquid interface(i.e. x direction) reads:

$$\mathbf{F}(x|t) = 2\pi\phi_a \left[a^\gamma \int_{|x-y|>a} \frac{(y-x)n(y|t)}{|x-y|^\gamma} dy + \int_{|x-y|\leq a} (y-x)n(y|t) dy \right] \quad (3)$$

Unlike Direct simulation Monte-Carlo (DSMC) for Boltzmann equation, where collision are local (same computing cell), the colliding partners are chosen as follows:

- a particle is chosen for collision based on the collision probability
- then the collision partner can therefore be chosen by drawing a random vector \hat{k} on the unit sphere and an elastic collision is applied

Kinetic theory approach to evaporation processes



- The vapor is described by the **Boltzmann** equation with a phenomenological boundary condition at the liquid-vapor interface.
- In case of *evaporation into vacuum*, the classical boundary condition reads:

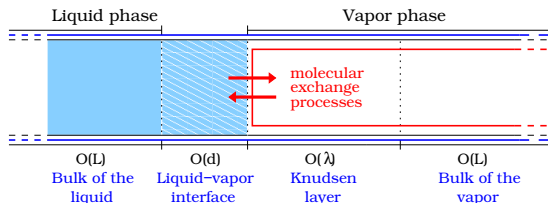
$$f(0, \mathbf{v}) = \alpha_e n_v(T_L) \left(\frac{1}{2\pi RT_L} \right)^{3/2} \exp\left(-\frac{\mathbf{v}^2}{2RT_L} \right), \quad v_{\perp} > 0,$$

T_L : temperature of the bulk liquid;

$n_v(T_L)$: saturated vapor density;

α_e : evaporation coefficient.

Kinetic theory approach to evaporation processes



- The boundary conditions assumed at the liquid-vapor have been extensively investigated by using molecular dynamics simulations^{1,2}.
- Unlike the Boltzmann equation, the Enskog-Vlasov equation has the capability of handling both the liquid and vapor phases^{3,4,5}:

¹ V.V. Zhakhovskii, S.I. Anisimov, *JETP* 84 (4), 734-745 (1997).

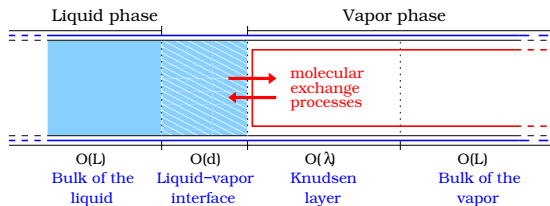
² T. Ishiyama, T. Yano, S. Fujikawa, *Phys. Fluids* 16 (8), 2899-2906 (2004).

³ A. Frezzotti, L. Gibelli, S. Lorenzani, *Phys. Fluids* 17, 012012 (2005).

⁴ M. Kon, K. Kobayashi, M. Watanabe, *Phys. Fluids* 26, 072003 (2014).

⁵ A. Frezzotti, L. Gibelli, D.A. Lockerby, J.E. Sprittles, *Phys.Rev. Fluids* 3, 054001 (2018).

Kinetic theory approach to evaporation processes



Usual distribution assumed:

$$\text{Undrifted Anisotropic: } f(v_{\parallel}, v_{\perp}) = \frac{C_1}{(2\pi R)^{3/2} \theta_{\perp} \theta_{\parallel}^{1/2}} \exp \left[-\frac{v_{\perp}^2}{2R\theta_{\perp}} - \frac{v_{\parallel}^2}{2R\theta_{\parallel}} \right], \quad v_{\perp} > 0,$$

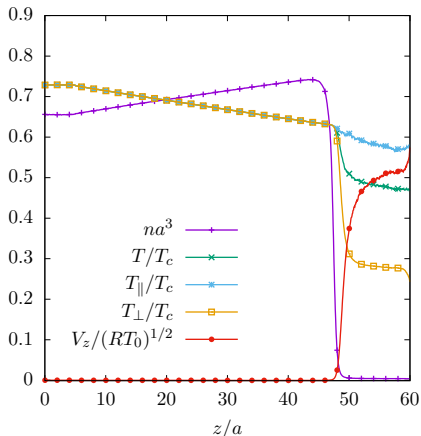
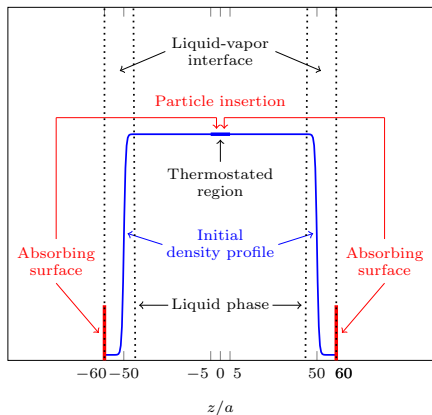
Proposed distribution:

$$\text{Drifted Anisotropic: } f(v_{\parallel}, v_{\perp}) = \frac{C_2}{(2\pi R)^{3/2} \theta_{\perp} \theta_{\parallel}^{1/2}} \exp \left[-\frac{(v_{\perp} - \xi)^2}{2R\theta_{\perp}} - \frac{v_{\parallel}^2}{2R\theta_{\parallel}} \right], \quad v_{\perp} > 0,$$

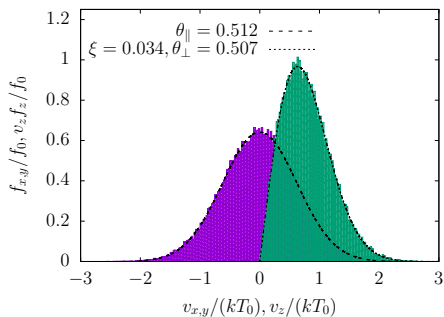
where C_i are constants used to normalise the velocity distribution functions.

Evaporation into near vacuum conditions

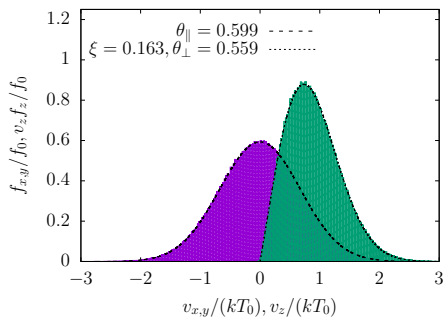
- The evaporation of a single-component liquid slab into near vacuum conditions has been studied.
- Goal: describe the origin of temperature anisotropy in the distribution of evaporated molecules



Velocity distribution functions



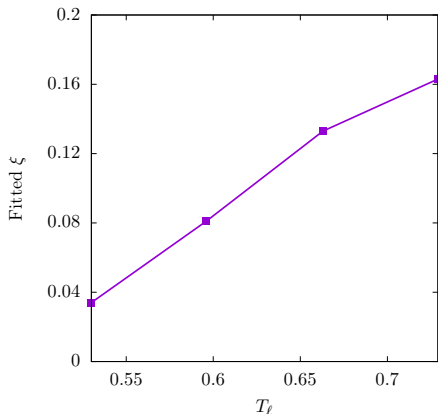
(a) $T_{\ell}/T_c = 0.53$



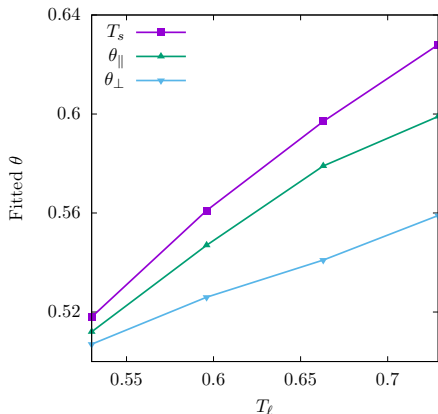
(b) $T_{\ell}/T_c = 0.729$

Figure: Reduced normalised velocity distribution functions of evaporated molecules normal and parallel to the liquid-vapor interface at different liquid bulk temperatures. Coloured histograms are the numerical results of the Enskog-Vlasov equation; solid and dashed lines are their best fits based on a drifted anisotropic Maxwellian with parameters θ_{\parallel} , θ_{\perp} , and ξ .

Velocity drift and temperature anisotropy



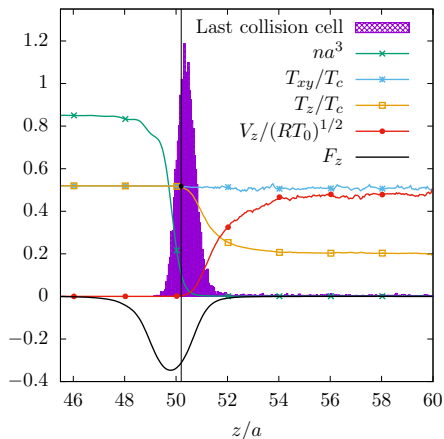
(a) Velocity drift.



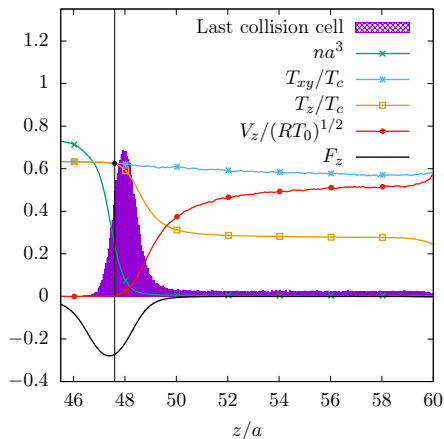
(b) Normal and parallel temperatures.

Figure: Parameters of the velocity distribution function of spontaneously evaporating atoms as a function of the liquid bulk temperature. The increasing trend of the the velocity drift and the temperature anisotropy with the liquid bulk temperature can be clearly observed.

Temperature anisotropy



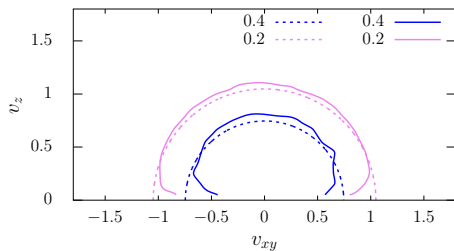
(a) $T_\ell/T_c = 0.53$



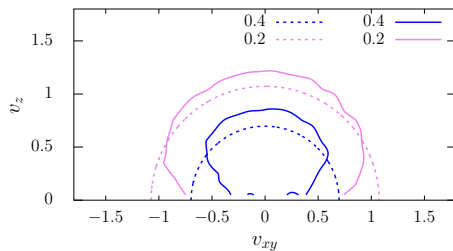
(b) $T_\ell/T_c = 0.729$

Figure: Histogram of the last collisional cell of evaporated particles for the smallest and largest liquid bulk temperatures considered in the simulation campaign. The peak of the distribution is close to the separation point which is marked by the vertical black line. The mean force field F_z is scaled down by a factor 10.

Temperature anisotropy



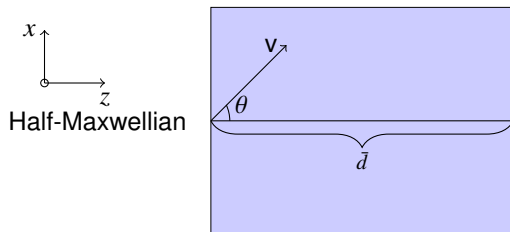
(a) $T_\ell/T_c = 0.53$



(b) $T_\ell/T_c = 0.729$

Figure: Isocontours of the distribution functions of evaporated atoms (dashed lines) and "potentially" evaporating atoms (solid lines). Atoms originate from locations before the separation point.

Toy model for the spontaneous evaporation



- We assume a Poisson distribution of the number of collisions at a collision rate $\bar{\nu}$:

$$Pr(N \text{ Collisions in the time interval } \Delta t) = \frac{(\bar{\nu}\Delta t)^N e^{-\bar{\nu}\Delta t}}{N!} \quad (4)$$

- Collision rate $\bar{\nu}$ is evaluated using the average of number density \bar{n} and temperature \bar{T} between the separation point and the absorption plane (this distance will be called \bar{d}):

$$\bar{\nu}(v) = \chi(\bar{n}) \frac{\pi a^2 \bar{n}}{\sqrt{\pi} \beta} \left[e^{-\beta^2 v^2} + \left(2\beta v + \frac{1}{\beta v} \right) \frac{\pi}{2} \operatorname{erf}(\beta v) \right], \quad (5)$$

where $\beta^2 = 1/(2R\bar{T})^3$.

Toy model for the spontaneous evaporation

- Particles need to have a velocity sufficiently large to overcome the potential barrier of the mean force field. This is modelled as the potential jump between a gas system of length \bar{d} and number density \bar{n} and vacuum.

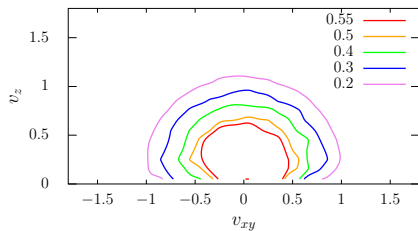
We are interested in the distribution of particles that do not collide:

$$Pr(N = 0) = e^{-\bar{v}t} = e^{-\bar{v}\frac{\bar{d}}{v_{\perp}}} \quad (6)$$

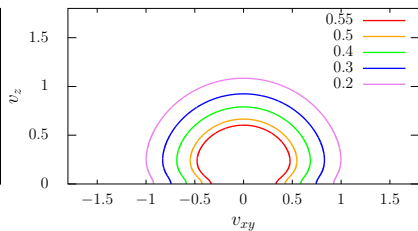
The distribution function of particles collected at the absorbing plate is found to be:

$$f_e(\tilde{v}_{\parallel}, \tilde{v}_{\perp}) = \frac{n_s}{(2\pi RT_s)^{3/2}} \exp\left(-\frac{\tilde{v}_{\perp,min}^2}{2RT_s}\right) \exp\left(-\frac{\tilde{v}_{\parallel}^2 + \tilde{v}_{\perp}^2}{2RT_s}\right) \exp\left(-\frac{\bar{v}\bar{d}}{\sqrt{\tilde{v}_{\perp}^2 + v_{\perp,min}^2}}\right) \quad (7)$$

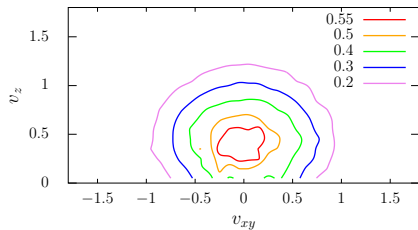
Toy model



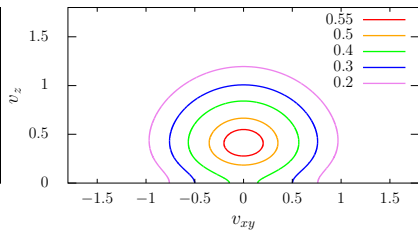
(a) Enskog-Vlasov solution, $T_\ell/T_c = 0.53$



(b) Toy model prediction, $T_\ell/T_c = 0.53$



(c) Enskog-Vlasov solution, $T_\ell/T_c = 0.729$



(d) Toy model prediction, $T_\ell/T_c = 0.729$

- The Enskog-Vlasov (EV) equation has been used to study the one-dimensional steady evaporation of a monatomic liquid into near vacuum conditions.
- Evaporated atoms are distributed according to a drifted anisotropic half-Maxwellian. Deviations from the isotropic half-Maxwellian become more pronounced as the liquid bulk temperature increases.
- The velocity drift and the temperature anisotropy are the results of collisions in the liquid-vapor interface region which preferentially backscatter atoms with a lower normal-velocity component. This statement is reinforced using a simple mathematical model.

- The Larsen-Borgnakke model is used for the redistribution between rotational and translational modes during inelastic collisions.
- The procedures of this model set the post-collision internal energies to values that satisfy the detailed balance principle.
- In this model the rotation energy adjustment is applied to a fraction of the total collisions, denoted $z_c = N_{coll}^{inelastic} / N_{coll}$.
- The strength of translational-rotational coupling is determined by the inelastic collision fraction z_c , which can be made to depend on the local flowfield temperature to fit experimental data⁵.

The Enskog-Vlasov equation

The evolution of the one-particle distribution function f of classical rigid rotators having $j = 2$ (linear molecule) or $j = 3$ (non-linear molecule) rotational degrees of freedom is given by:

$$\frac{\partial f}{\partial t} + \mathbf{v} \cdot \nabla_{\mathbf{r}} f + \underbrace{\frac{\mathbf{F}(\mathbf{r})}{m} \cdot \nabla_{\mathbf{v}} f}_{\text{Vlasov term}} = \underbrace{\mathbf{C}(f, f)}_{\text{Enskog term}}$$

$$\mathbf{F}(\mathbf{r}) = \int_{r>a} d\mathbf{r}_* \frac{1}{r} \frac{d\phi}{dr} (\mathbf{r}_* - \mathbf{r}) n(\mathbf{r}_*),$$

$$\mathbf{C}(f, f) = \int d\epsilon_* d\mathbf{v}_* d^2 \hat{\mathbf{k}} (\mathbf{v}_r \cdot \hat{\mathbf{k}})^+ \mathbf{Q} \epsilon_*^\mu \left\{ \chi[\bar{n}(\mathbf{r} - a/2\mathbf{k})] f(\mathbf{r}, \mathbf{v}') f(\mathbf{r} + a\hat{\mathbf{k}}, \mathbf{v}'_*) - \chi[\bar{n}(\mathbf{r} - a/2\mathbf{k})] f(\mathbf{r}, \mathbf{v}) f(\mathbf{r} - a\hat{\mathbf{k}}, \mathbf{v}_*) (\mathbf{v}_r \cdot \hat{\mathbf{k}}) \right\}.$$

(8)

The Enskog-Vlasov equation

Q is defined as:

$$Q = \int_S d^2 \hat{e}' \int_0^E d\epsilon' \epsilon'^{\mu} \int_0^{E-\epsilon'} d\epsilon'_* \epsilon'^{\mu} \frac{v_r'^2}{v_r} \sigma(\epsilon', \epsilon'_* \rightarrow \epsilon, \epsilon_*; E, \hat{e}' \cdot \hat{e}).$$

where $\sigma(\epsilon', \epsilon'_* \rightarrow \epsilon, \epsilon_*; E, \hat{e}' \cdot \hat{e})$ is the differential cross-section associated with the binary collision of a pair of molecules in the initial states (\mathbf{v}', ϵ') , $(\mathbf{v}'_*, \epsilon'_*)$ that move to the final states (\mathbf{v}, ϵ) , $(\mathbf{v}_*, \epsilon_*)$; $\hat{e} = \mathbf{v}_r/v_r$ and $\hat{e}' = \mathbf{v}'_r/v'_r$ are unit vectors with the direction of the relative velocities $\mathbf{v}_r = \mathbf{v}_* - \mathbf{v}$ and $\mathbf{v}'_r = \mathbf{v}'_* - \mathbf{v}'$; E is the total energy of the collision pairs in the center of mass reference frame.

The selection of the collision partners follows the same procedure as described by Frezzotti⁶, while the collision dynamics can be summarized as follows:

- A collision is inelastic with probability z_c or elastic with probability $1 - z_c$.
- In an elastic collision, the rotational energies of the two colliding partners do not change, such that $\varepsilon = \varepsilon'$ and $\varepsilon_* = \varepsilon'_*$. Conservation of total energy leads to $v_r = v'_r$ and the post-collision relative velocity is given by $\mathbf{v}_r = v_r \hat{\mathbf{e}}$, with $\hat{\mathbf{e}}$ a random vector uniformly distributed on a unit sphere.

Larsen-Borgnakke model: numerical scheme (II)

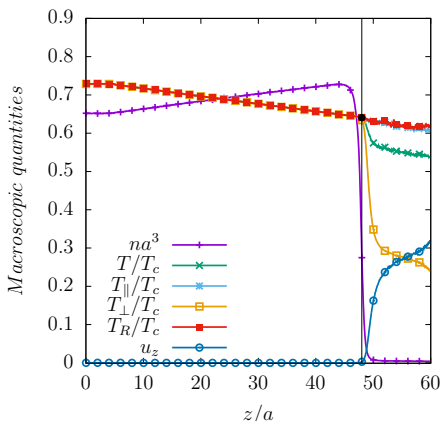
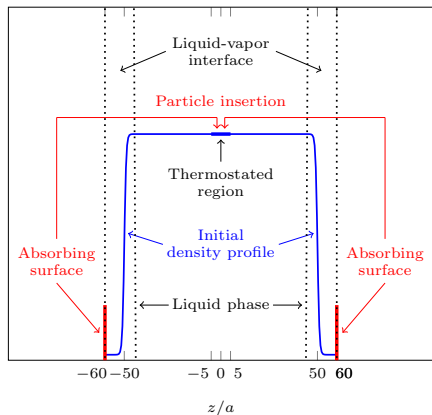
- In an inelastic collision, an exchange between translational and rotational energies occurs as follows:
 - the translational energy E_{tr}/E is sampled from the probability density $\mathcal{P}_t(E_{tr}/E; j)$.
 - the remaining total rotational energy $E_{rot} = E - E_{tr}$ is then divided between the collision partners by sampling the fraction ε/E_{rot} from the probability density $\mathcal{P}_r(\varepsilon/E_{rot}; j)$.
 - the post-collision relative velocity is updated to $\mathbf{v}_r = v_r(E_{tr})\hat{\mathbf{e}}$, with $v_r(E_{tr}) = \sqrt{4E_{tr}/m}$.

$$\mathcal{P}_t(E_{tr}/E; j = 2) = 4 \frac{E_{tr}}{E} \left(1 - \frac{E_{tr}}{E}\right), \quad \mathcal{P}_r(\varepsilon/E_{rot}; j = 2) = 1,$$

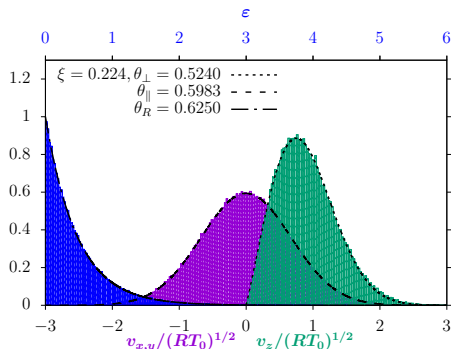
$$\mathcal{P}_t(E_{tr}/E; j = 3) = \frac{27}{4} \frac{E_{tr}}{E} \left(1 - \frac{E_{tr}}{E}\right)^2, \quad \mathcal{P}_r(\varepsilon/E_{rot}; j = 3) = 2 \sqrt{\frac{\varepsilon}{E_{rot}} \left(1 - \frac{\varepsilon}{E_{rot}}\right)}.$$

Evaporation into vacuum

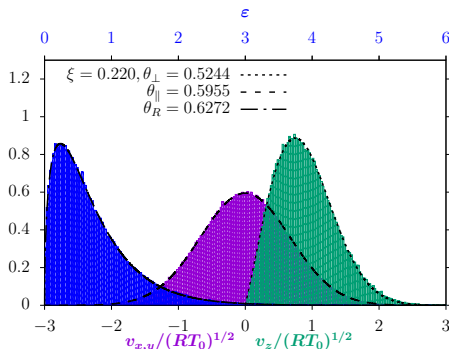
- The Enskog-Vlasov equation has been solved numerically by an extension of Direct Simulation Monte Carlo (DSMC) method to dense polyatomic fluids.
- The simulation campaign is carried out for temperatures in the range $T_\ell/T_c = [0.53, 0.729]$ and for values spanning the entire range $z_c \in [0, 1]$, for both $j = 2$ and $j = 3$.



Evaporated molecules: Distribution functions



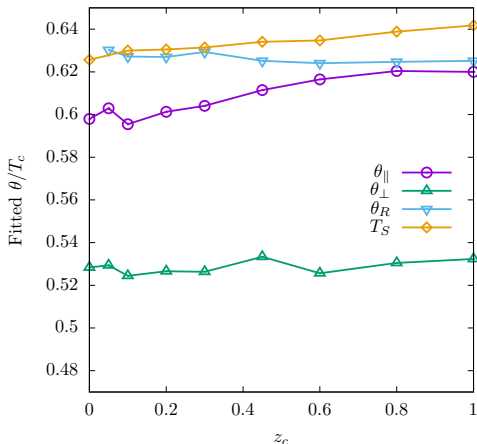
(a) $j = 2$



(b) $j = 3$

Reduced velocity distribution function and molecular flux, parallel (violet) and normal (green) to the liquid-vapor interface, respectively, and rotational energy distribution (blue) of evaporated molecules, at $T_{\ell}/T_c = 0.729$ liquid bulk temperature, for (a) linear ($j = 2$) and (b) nonlinear ($j = 3$) molecules, and inelastic collision fraction equal to unity ($z_c = 1$). The dashed lines are the best fits based on the drifted anisotropic Maxwellian with parameters ξ , θ_{\perp} , θ_{\parallel} and the Boltzmann distribution with parameter θ_R .

Evaporated molecules: Distribution functions



(a) $T_{\ell}/T_c = 0.729$

Fitted temperatures versus the inelastic collision fraction z_c for non-linear molecules ($j = 3$) at the highest liquid bulk temperatures T_{ℓ} considered.

- The Enskog-Vlasov equation has been extended to deal with polyatomic substances composed of classical rigid rotators.
- The translational velocities of evaporated molecules are distributed according to a half-range drifted anisotropic Maxwellian.
- The rotational energy of evaporated molecules is distributed according to the Boltzmann distribution at a temperature θ_R which depends on the inelastic collision fraction z_c , namely:
 - The separation temperature T_s (low values of z_c).
 - The parallel temperature θ_{\parallel} (high values of z_c).

Weighted scheme for spherically symmetric EV

The aim of this research is to develop a weighted particle scheme for solving the Enskog-Vlasov equation in spherical geometry. This required a special treatment of the collision mechanism as well as an efficient way to evaluate the mean-field in spherical coordinates.

The evolution equation of the one-particle distribution in spherical coordinates with spherical symmetry reads:

$$\frac{\partial f}{\partial t} + v_r \frac{\partial f}{\partial r} + \left(\frac{\mathcal{F}_r[n]}{m} - \frac{v_r^2}{r} \right) \frac{\partial f}{\partial v_r} = C_E[f], \quad (9)$$

where $\mathcal{F}_r[n]$ is the radial component of the self-consistent force field generated by the soft attractive tail, which depends on the number density field $n(r, t)$, and $C_E[f]$ is the hard-sphere collision integral (square brackets are used to highlight the functional dependence).

Self-consistent force field - Illustration

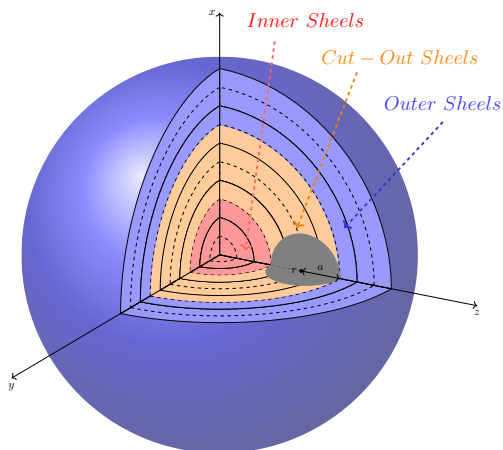


Figure: Radial component of the self-consistent force field evaluation. The spherical shells are partitioned into 3 groups: the inner shells (11), the outer shells (12) and the cutout spherical shells (13). The cut out sphere of radius a has the origin on the cell center and, subsequently, the edges on a cell center.

The general expression of the self-consistent force field generated by the soft attractive tail is given by:

$$\mathcal{F}[n] = \int_{\|\mathbf{r}_1 - \mathbf{r}\| > a} \frac{d\phi_a(\rho)}{d\rho} \frac{\mathbf{r}_1 - \mathbf{r}}{\|\mathbf{r}_1 - \mathbf{r}\|} n(\mathbf{r}_1) d\mathbf{r}_1. \quad (10)$$

Inner whole shells contribution:

$$\begin{aligned} \mathcal{F}_r(r|t) = & 2\pi\phi_a a^6 \int_{(r-R)>a} \left[\frac{(r^2 - R^2)^{-\gamma} (-(r-R)^\gamma (r+R)^2 + (r-R)^2 (r+R)^\gamma)}{\gamma - 2} \right. \\ & \left. + \frac{r^2 ((r-R)^{-\gamma} - (r+R)^{-\gamma})}{\gamma} + \frac{R^2 (-(r-R)^{-\gamma} + (r+R)^{-\gamma})}{\gamma} \right] \frac{n(R|t) dR}{r^2} \quad (11) \end{aligned}$$

Outer whole shells contribution:

$$\mathcal{F}_r(r|t) = 2\pi\phi_a a^6 \int_{(r-R)<a} \left[\frac{(R^2 - r^2)^{-\gamma} (-(R-r)^\gamma (r+R)^2 + (r-R)^2 (r+R)^\gamma)}{\gamma - 2} + \frac{r^2 ((R-r)^{-\gamma} - (r+R)^{-\gamma})}{\gamma} + \frac{R^2 (-(R-r)^{-\gamma} + (r+R)^{-\gamma})}{\gamma} \right] \frac{n(R|t) dR}{r^2} \quad (12)$$

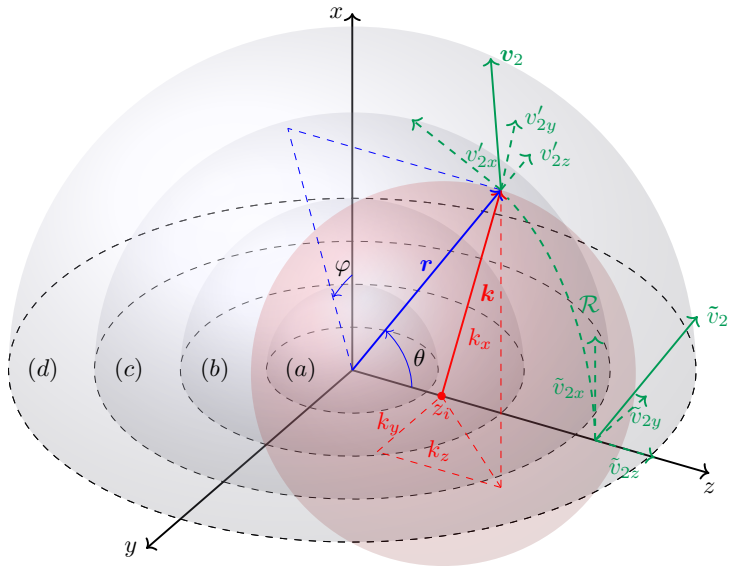
Cut-out shells contribution:

$$\mathcal{F}_r(r|t) = 2\pi\phi_a a^6 \left[\int_{|r-R|\leq a} \left[-2a^\gamma (r+R)(R+r(\gamma-1)) + (r-R)(r+R)^{1+\gamma}(\gamma-2) + a^2 \gamma (r+R)^\gamma \right] \times \frac{3R}{r^2} \frac{(a(r+R))^{-\gamma}}{(\gamma-2)\gamma} n(R|t) dR \right] \quad (13)$$

The radial component of the self-consistent force field obtained for $\gamma = 6$:

$$\mathcal{F}_r[n(r, t)] = 2\pi\phi_a a^6 \left[\int_{|r-R|>a} \frac{4(3r^3 R^2 + 5rR^4)n(R, t)}{(R-r)^5(R+r)^5} dR + \int_{|r-R|\leq a} \frac{R}{4r^2} \left(\frac{3}{a^4} + \frac{2(R-r)(R+r)}{a^6} - \frac{5r+R}{(R+r)^5} \right) n(R, t) dR \right] \quad (14)$$

Collision process



Validation - Fluid surface tension

T/T_c	Planar ⁸	Cylindrical ⁴	Spherical
0.729	0.184	0.178	0.180
0.795	0.123	0.121	0.118
0.861	0.0698	0.0675	0.068

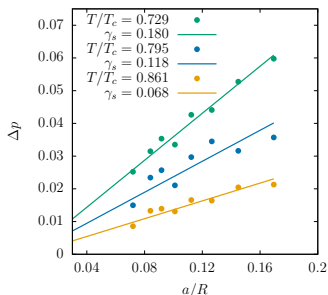


Figure: Validation case study I: Pressure difference at the liquid-vapor interface, ΔP , versus the reciprocal of the droplet radius, $1/R$, for different temperatures.

Validation - Droplet critical radius

According to the classical nucleation theory (CNT), the critical radius, R^* , is given by:

$$R^* = \frac{2\gamma}{n_\ell k_B T \ln S} \quad (15)$$

where n_ℓ is the equilibrium liquid number density at the temperature T , and $S = p(T, n_v)/p(T)$.

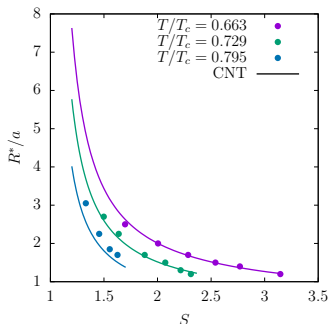
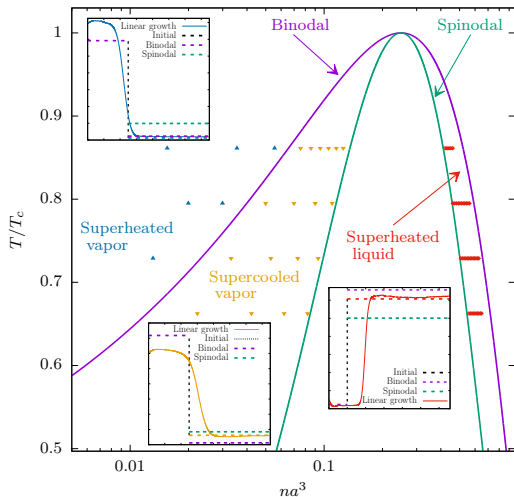


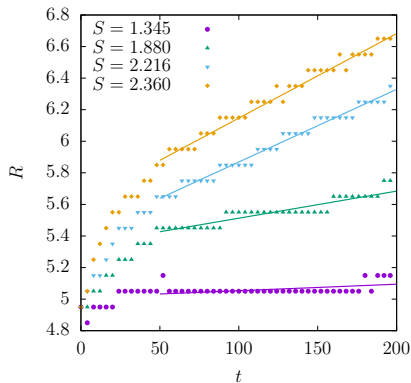
Figure: Dimensionless critical radius, R^*/a , versus the supersaturation ratio S for different values of the temperatures.

Phase diagram

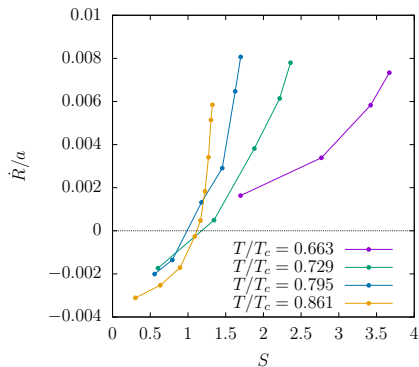


Phase diagram. Solid symbols represent the initial conditions of the simulation campaign carry out to evaluate the growth rate of droplets and bubbles.

Growth of liquid droplets in metastable vapor



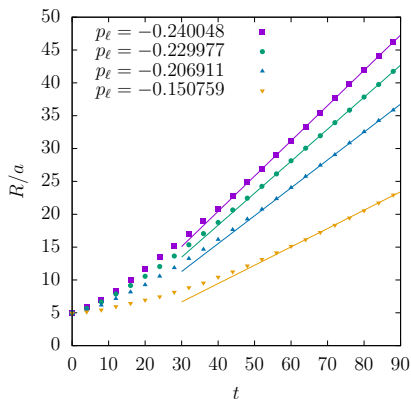
(a) Bulk temperature evolution



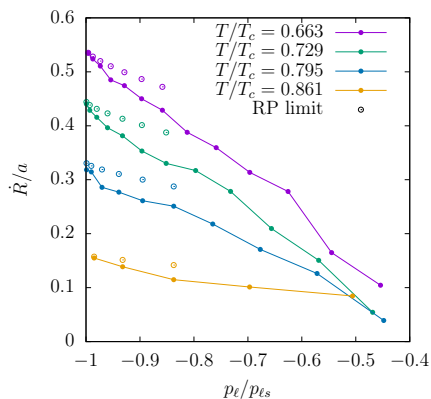
(b) Average droplet growth

Figure: (a) Typical growth curves for $T_0/T_c = 0.729$ and a series of supercooling ratios S , with the corresponding best linear fit lines. (b) Average droplet growth rate \dot{R} with respect to the supercooling ratio $S = p(T, n_v)/p(T)$ for $T/T_c = 0.663; 0.729; 0.795; 0.861$.

Growth of bubbles in superheated liquid - growth rate



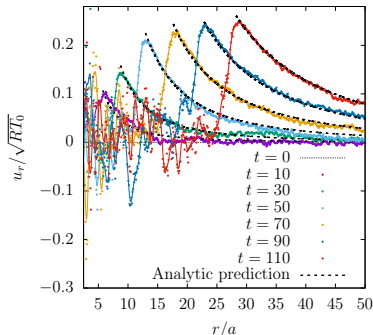
(a) $T_0/T_c = 0.663$



(b) Average bubble growth

Figure: (a) Typical growth curves for $T_0/T_c = 0.663$ and a series of liquid pressures p_ℓ with the corresponding best linear fit lines. (b) Average bubble growth rate \dot{R} with respect to the surrounding liquid pressure $p_\ell/|p_{\ell s}|$, normalised to the value of the pressure on the spinodal line $p_{\ell s}$.

Growth of bubbles in superheated liquid - radial velocity

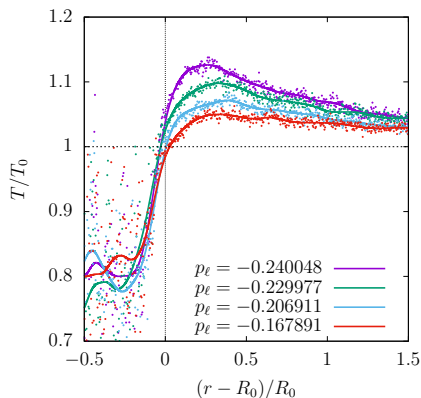


Radial macroscopic velocity profiles during bubble growth at $T_0/T_c = 0.729$ and $p_\ell = -0.1098$. The dashed analytic curves obtained following the model proposed by Vincent and Marmontant⁹:

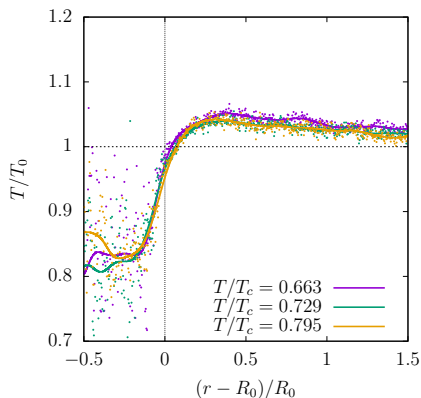
$$u(r) = \frac{n_\ell - n_v}{(n_\ell - x^3 n_v)} \frac{x^2}{1 - x^3} \dot{R} \left[\frac{R_w^2}{r^2} - \frac{r}{R_w} \right] \quad (16)$$

where $x = R/R_w$.

Growth of bubbles in superheated liquid - Temperature



(a)



(b)

- (a) Temperature profiles during bubble growth at $T_0/T_c = 0.663$ and $R_0 = 25a$. (b) Temperature profiles during bubble growth at $T_0/T_c = \{0.663, 0.729, 0.861\}$ and $\dot{R} \approx 0.3$. R_0 is the position of the interface.

- The EV equation is solved for the first time in spherical geometry using a weighted particle scheme. The collision dynamics between weighted particles has been derived accounting for the non-locality of the Enskog collision term, and a compact expression of the Vlasov mean force field has been determined using the shell theorem.
- An extensive simulation campaign was then carried out to investigate the growth of droplets and bubbles in metastable vapor and superheated liquid, respectively.
- The scheme is to be used to study the distribution function of evaporated molecules with respect to the radius of the droplet

Thank you for your attention